Quick estimates for analysis and prediction of the flight mechanics of unmanned aerial vehicles

Mark Müller,[a] Leon Liebenberg (corresponding author),[b] Edward H. Mathews[b] and Peter W. Young[c]

[a] *Institute for Dynamic Systems and Control, ETH Zurich, ML K32.3, Sonneggstrasse 3, 8092 Zürich, Switzerland*

[b] *Center for Research and Continued Engineering Development, North-West University (Pretoria campus), Suite no. 93, Private Bag X30, Lynnwood Ridge 0040, South Africa. Consultants to TEMM Intl. (Pty) Ltd*
E-mail: LLiebenberg@researchtoolbox.com

[c] *The Aerospace Corporation, PO Box 92957, Los Angeles, CA 90009-2957, USA*

Abstract   Unmanned aerial vehicles (UAVs) are commonly employed in undergraduate engineering curricula. Limited literature is, however, available for the lay design engineer or engineering student regarding the modelling, simulation and analysis of the flight dynamics of small UAV systems, especially pertaining to flight dynamics modelling. There is great demand for unskilled UAV designers to predict the stability of new designs, quickly, cheaply, and with relative ease, preferably during the conceptual design stage. This paper summarizes some salient techniques for performing quick characterization of the longitudinal dynamics of a small, electrically propelled UAV, by using freely available software such as Datcom+, AVL, XFLR5 and MotoCalc. The simulation outputs compare favourably with experimental results from a wind tunnel. The software was also used to provide accurate estimates of coefficients required for performing an analysis of the UAV's longitudinal dynamics. The proffered analytical techniques should greatly benefit lay design engineers and engineering students venturing into the realm of UAV research.

Keywords   unmanned aerial vehicles (UAVs); longitudinal dynamics; quick characterization

Notation

A	main wing aspect ratio [–]
A_t	horizontal tail aspect ratio [–]
a_w	lift-curve slope for main wing [rad^{-1}]
a_t	lift-curve slope for horizontal tail [rad^{-1}]
b	main wing span [m]
c	airfoil chord [m]
$\overline{c}$	wing mean aerodynamic chord [m]
C_X	coefficient of some force/moment X
C_{X_Y}	derivative of C_X with respect to Y, i.e. $\partial C_x/\partial Y$
$C_{X(A)}$	component of C_X due to aerodynamic forces [–]
$C_{X(T)}$	component of C_X due to thrust forces [–]
D	drag force [N]
D_0	base drag force [N]
D_i	induced drag force [N]

D_{prop} propeller diameter [m]
e Oswald's efficiency factor [–]
E_{bat} battery energy capacity [J]
g gravitational acceleration [m/s^2]
h aircraft height above sea level [m]
I_y mass moment of inertia about y-axis [kg.m^2]
l aerofoil sectional-lift [*N/m*]
l_{p} distance between propeller and UAV centre of gravity [m]
l_{t} distance between horizontal tail neutral point and UAV centre of gravity [m]
l_{w} distance between main wing neutral point and UAV centre of gravity [m]
$\bar{m}$ UAV mass [kg]
m pitching moment [Nm]
M Mach number [–]
n propeller rotational speed [min^{-1}]
P power [W]
q dynamic pressure [Pa]
R range [m]
Re Reynolds number [–]
S main wing planform area [m^2]
S_{D} propeller disk area [m^2]
S_{t} horizontal tail planform area [m^2]
T thrust force [N]
u UAV airspeed [m/s]
V speed [m/s]
$\bar{V}_{\text{h}}$ horizontal tail volume coefficient [–]
$X, Z_{\text{subscript}}$ linear dimensional stability derivatives [–]
x_{cg} distance to centre of gravity, from reference point [m]
x_{n} distance to UAV neutral point, from reference point [*m*]
x_{nt} distance to horizontal tail neutral point, from reference point [m]
x_{nw} distance to main wing neutral point, from reference point [m]
α angle of attack [rad]
δ_{e} elevator deflection [rad]
Δt rotation period [s]
ε_{α} rate of change of the downwash angle at the horizontal tail with change in α [–]
γ flight path angle [rad]
η_{t} horizontal tail efficiency [–]
η_{p} propulsion system efficiency [–]
θ pitch angle [rad]
θ_{T} thrust angle with respect to reference line [rad]
ρ air density [kg/m^3]
υ kinematic viscosity [m^2/s]
$\bar{\omega}$ natural frequency [rad/s]
ς damping ratio [–]

Introduction

Airplane flight dynamics models are extensively used for simulation, implementation of flight control law algorithms, and extraction of low-order models for flight control synthesis. Such dynamics models therefore lower the cost and risk associated with the design and operation of the real airplane system [1–7]. Modelling, simulation and analysis, and flight testing of large airplanes are very well established. However, limited literature is available for the lay design engineer or engineering student regarding the modelling, simulation and analysis of the flight dynamics of small unmanned aerial vehicle (UAV) systems, especially pertaining to flight dynamics modelling [8].

Additionally, there is a growing demand for reliable and low-cost UAV systems. This is especially true for mini-UAV systems (with wing spans of up to around 2 m), where the majority of such airplanes are still deployed as prototypes due to their lack of reliability [9]. Improvement in the modelling, testing and flight control for small UAVs would increase their reliability during autonomous flight [10].

An experimental, low-cost mini-UAV (Fig. 1) was designed and built at the University of Pretoria's Department of Mechanical and Aeronautical Engineering [11]. The UAV was designed for wildlife surveillance, and as such has a payload bay in which a camera is mounted. A primary design goal was flight endurance of at least 45 minutes, which largely determined the design of the electrical drive system. The UAV is launched by hand, and lands on the belly of the payload unit.

One objective of the study was to create a method for unskilled UAV designers to predict the stability of new designs, quickly, cheaply, and with relative ease, preferably during the conceptual design stage.

The proof-of-concept UAV was subjected to testing in a wind tunnel, and also to limited real-world experiments (under remote control). The salient characteristics of this mini-UAV are provided in Table 1 and Fig. 2.

This paper shows how lay mini-UAV designers and engineering students could investigate such an airplane's longitudinal dynamic stability. Although the equations of motion for a fixed-wing aircraft are well known [1, 3, 4–7], difficulties arise from
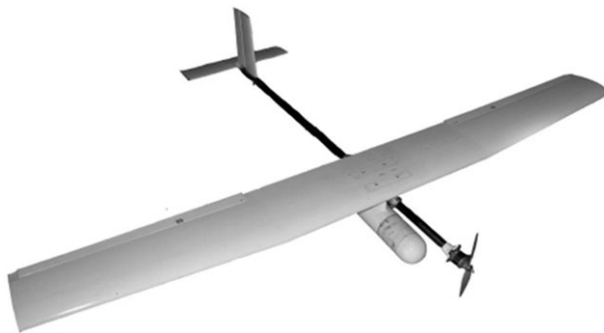

Fig. 1   *The experimental UAV of the University of Pretoria [11].*

TABLE 1   *Salient characteristics of the experimental UAV*

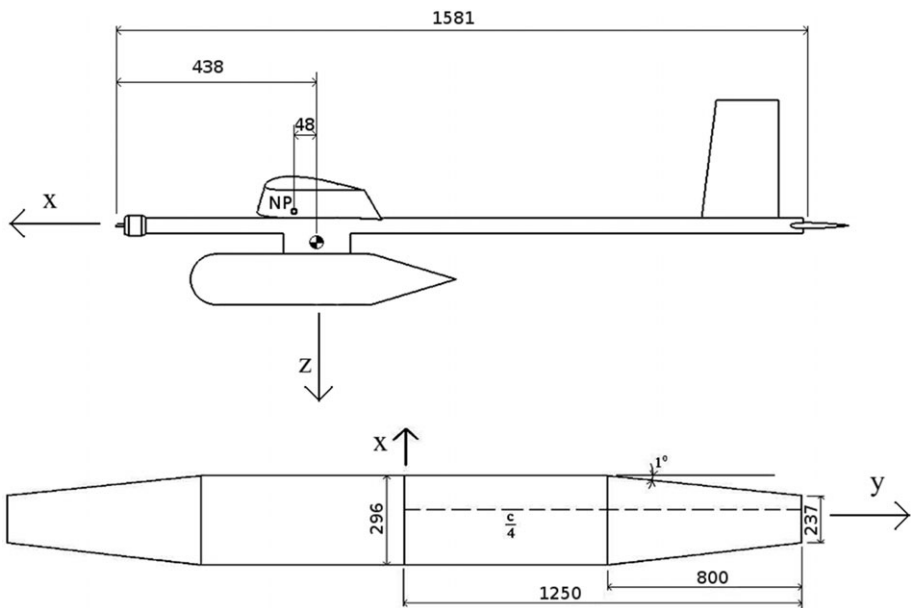| Characteristic	Value
Mass	$\bar{m} = 5.3$ kg
Main wing span	$b = 2.5$ m
Main wing area	$S = 0.6928$ m^2
Cruising speed	$V_{cruise} = 18$ m/s
Propulsion system	12″ × 6″ (304 mm × 152 mm) propeller, 500 W brushless motor, two 3-cell Li-Po battery packs (6 × 3.7 V) giving 14.8 V and 6000 mAh
Reynolds number (at cruise)	Re = 300,000

Fig. 2   *Important dimensions of the experimental UAV airframe, and main wing (below). Distances in mm, with the wing neutral point denoted by NP; the quarter-chord position (c/4) is also depicted.*

handling the aerodynamic forces and moments [12]. This is due to complex dependence of aerodynamic forces and moments on a number of variables. This results in complicated non-linear correlations between variables [12]. We describe relatively simple methods for predicting various parameters affecting the stability and performance of a mini-UAV, as well as a method for calculating the transfer functions that govern the (linearized) longitudinal motion. Apart from giving information on stability, these transfer functions can be used for autopilot design.

Dynamic characterization of the small UAV

Computer analyses

An airplane possesses dynamic stability if the amplitudes of any aperiodic and oscillatory motions induced by disturbances eventually decrease to zero relative to a steady-state flight condition [7]. To study dynamic stability, the authors analysed the well known differential equations of airplane motion. For small perturbations, these equations can be decoupled into longitudinal and lateral directional components, with three degrees of freedom in each [1–7]. Small-perturbation theory also allows the approximation of the actual non-linear differential equations as linear ones with constant coefficients, while ignoring any less significant non-linear aerodynamic effects.

Besides hand calculations, the aerodynamic properties of the UAV were analysed using freely available software, such as Datcom+ [13, 14], AVL (Athena Vortex Lattice) [15] and XFLR5 [16]. Datcom+ and AVL are used to analyse entire aircraft configurations, and XFLR5 is used for aerofoil analysis. Datcom+ is based on the USAF Stability and Control Data Compendium and uses a mixture of empirical and analytical methods to analyse fixed-wing aircraft, with the empirical data based on large aircraft operating at large Reynolds numbers [13, 14]. This means that the results for a small UAV should be treated with caution. AVL is an inviscid vortex lattice code which is used to analyse configurations of thin wings at small angles of attack and sideslip, as well as slender bodies [15], over a very wide range of Reynolds numbers [17–19]. No literature could be found that provides a lower limit on Reynolds number. AVL is presently the only freely available software that calculates stability derivatives.

Because the programs use different analytical approaches, a close agreement between them would be a strong indication of accurate estimates. Ideally, the results should be compared to wind tunnel test results as well [20–22], or computational fluid dynamics (CFD) analyses, to verify their applicability to flight at a lower Reynolds numbers.

The performance of the electric propulsion system was analysed using MotoCalc [23], a software program which predicts performance of the entire propulsion system, including battery, speed controller, motor and propeller.

Main wing

The planform area of a wing (S) is defined as the area seen if looking at the wing from directly above or below, while the span (b) is the distance measured on the planform from one wingtip to the other [24]. The aspect ratio, A, of the wing gives information on the shape of the planform, defined in equation 1, and is an important factor determining a three-dimensional wing's aerodynamic properties. Finally, the mean aerodynamic chord, $\bar{c}$, is a measure used to non-dimensionalize the pitching moment.
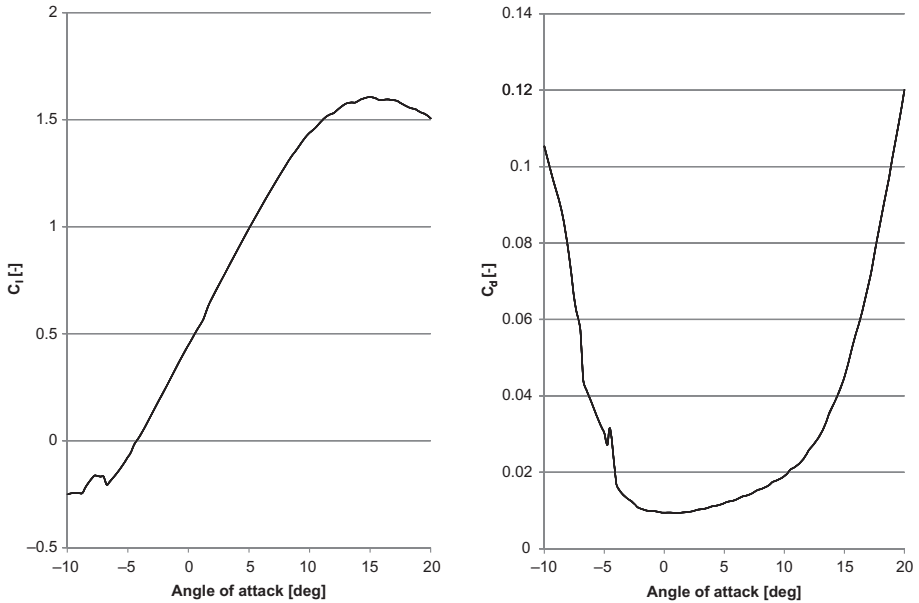
$$A = \frac{b^2}{S} \tag{1}$$

Fig. 3   *Lift/drag for the experimental UAV main-wing airfoil (SD7062), calculated using XFLR5 (which in turn uses XFoil). Note that the airfoil stalls at an angle of attack (α) of 15°. These results were calculated at the cruising Reynolds number of 300,000.*

$$\bar{c} = \frac{2}{S} \int_0^{b/2} c^2(y)\mathrm{d}y \tag{2}$$

Also of great importance to the aerodynamic properties of the wing is the aerofoil, or span-wise cross-section. Using thin-aerofoil theory, or software like XFLR5, the properties of an aerofoil can be estimated, and then used to generate a result for a three-dimensional wing. A parameter which has a great influence on the performance of the wing is the dimensionless Reynolds number, defined as Re = $V\bar{c}/v$ [25].

A lift/drag analysis of an aerofoil is shown in Fig. 3, from which important information can be found: first, the slope of the curve, C_{l_a}, in the linear regions (i.e. at small α) can be estimated. This can be compared with the theoretical result of $C_{l_a} = 2\pi \approx 6.28 / rad$ predicted by thin-aerofoil theory [24]. Furthermore, the sectional lift at zero angle of attack can be read off, while the stall point can be seen to be the point at which maximum lift occurs. The wing lift-curve slope, which is smaller for a finite wing than for an aerofoil, can be estimated as [24]:

$$a_{\mathrm{w}} \approx C_{l_\alpha}\left(\frac{A}{A+2}\right) \tag{3}$$

Horizontal stabilizer
The horizontal stabilizer, being a smaller lifting surface, is generally located relatively far behind the aircraft's centre of gravity (below, denoted subscript cg), and

is vital for longitudinal stability. The aircraft's elevator is usually a part of the, or the entire, horizontal stabilizer. Some important values associated with the horizontal stabilizer are the planform area (S_t), the lift-curve slope (a_t), the efficiency (η_t) and rate of change of the downwash angle with changing angle of attack (ε_α).

The planform area and lift-curve slope are determined in the same way as for the main wing [24]:

$$a_t \approx C_{l_\alpha(t)} \left(\frac{A_t}{A_t + 2} \right) \tag{4}$$

The horizontal tail efficiency, η_t, is defined as the ratio of local dynamic pressure at the horizontal tail to the free-stream dynamic pressure, which is influenced by factors such as flow deflections due to the wing/fuselage and propeller wash. This parameter is very difficult to estimate, and as it is usually close to unity it can be assumed that $\eta_t \approx 1$ [24].

The value $\varepsilon_\alpha = \delta\varepsilon/\delta\alpha$ can be estimated from empirical graphs, being a function of aspect ratio, wing lift-curve slope, wing span, and wing sweep [24]. Alternatively, a program such as Datcom can be utilized.

Neutral point

An aircraft's neutral point (below, denoted subscript n) is defined as the point about which the pitching moment is independent of angle of attack, related to the aerodynamic centre of an aerofoil [24]. The location of the neutral point is a very important parameter affecting the longitudinal stability of an aircraft [25].

An aircraft with the neutral point behind (i.e. downstream of) its centre of gravity is said to be statically unstable, while the aircraft is stable for the neutral point ahead of the centre of gravity. If the two points coincide, the aircraft is said to be neutrally stable. Static stability is a necessary condition for dynamic stability [24], discussed later.

If an aircraft experiences a slight upwards disturbance in angle of attack from steady flight, the total lift will also increase. Because the aircraft was initially in steady flight, the initial pitching moment is trimmed to zero. If the centre of gravity is located in front of the neutral point, the slight increase in lift will cause an opposing pitching moment, tending to restore the aircraft to its original flight condition. If the centre of gravity lies behind the neutral point, an increase in angle of attack will produce a pitching moment in the same direction as the original disturbance, causing a further increase in angle of attack, thus unstable behaviour (see Fig. 4).

The location of the neutral point of an aircraft can be calculated from equation 5 [24]:

$$x_n = \frac{x_{nw} + x_{nt}\eta_t \dfrac{S_t}{S} \dfrac{a_t}{a_w}(1-\varepsilon_\alpha)}{1+\eta_t \dfrac{S_t}{S} \dfrac{a_t}{a_w}(1-\varepsilon_\alpha)} \tag{5}$$
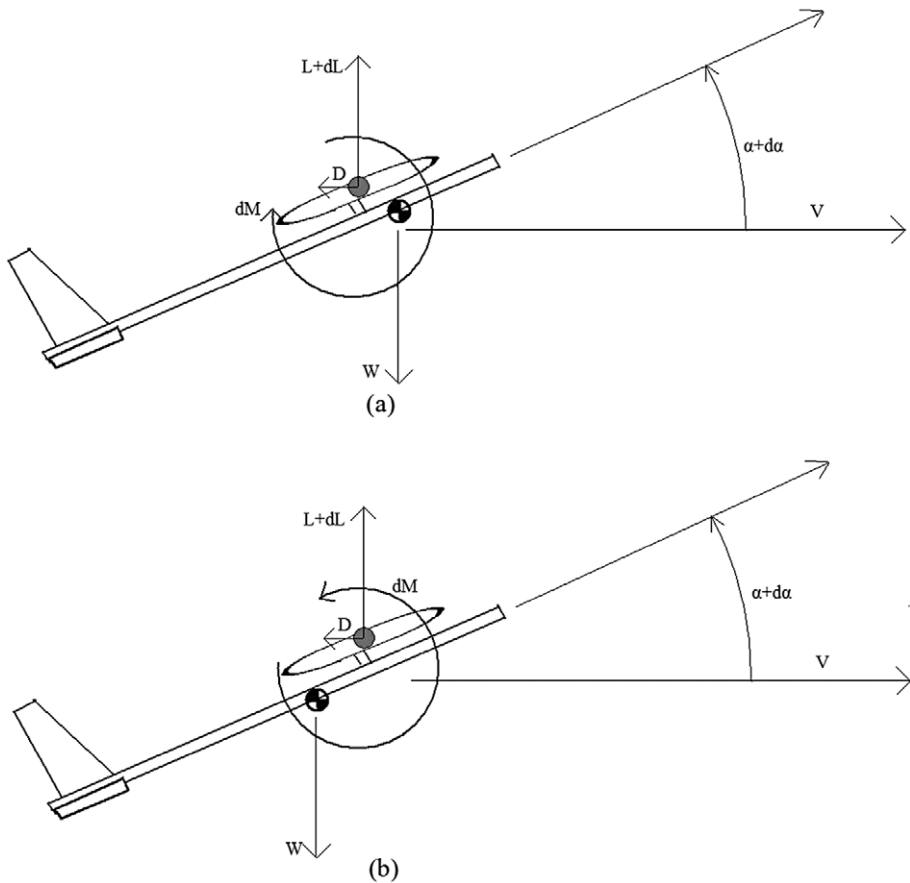
Fig. 4   *Statically stable (a) and unstable (b) configurations experiencing a perturbation in angle of attack from level flight, leading to restoring (a) and diverging (b) pitching moments.*

where x_n, x_{nw} and x_{nt} are distances of the aircraft's neutral point, the wing's neutral point and the horizontal stabilizer's neutral point, respectively, measured from some reference point. The neutral point for the lifting surfaces can usually be taken as lying on the quarter-chord of the airfoils [24, 25].

An indication of the relative static stability of an aircraft is given by the static margin (*SM*). The *SM* is the normalized distance between the centre of gravity and the neutral point [24, 25]:

$$SM = \frac{x_n - x_{cg}}{\bar{c}} \tag{6}$$

The *SM* is defined as being positive for statically stable aircraft, and a 'good' value lies somewhere in the range $0.07 < SM < 0.1$ [24, 25].
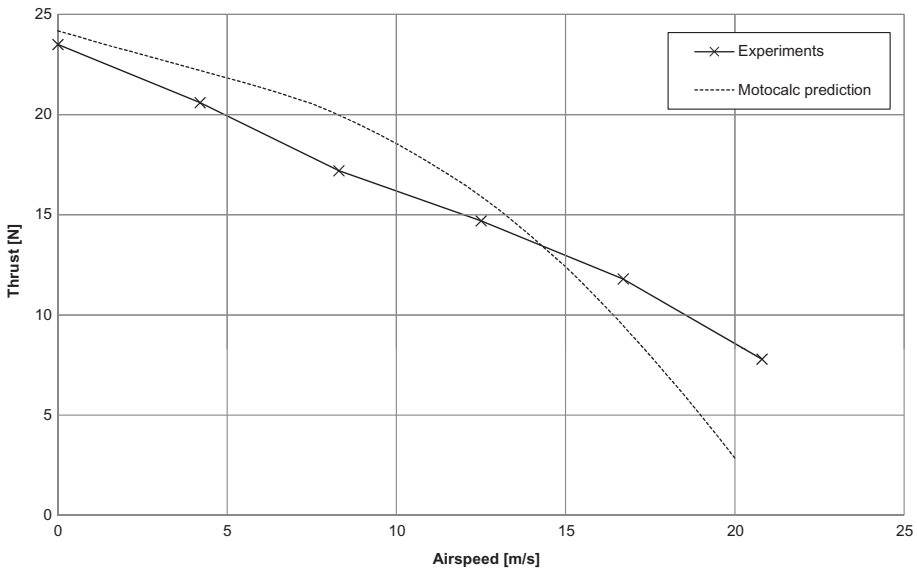
Fig. 5   *Experimental and MotoCalc-predicted thrust force, as functions of airspeed for the experimental UAV.*

Propulsion

The propulsion system of an electrically powered UAV consists of four main components: the propeller, motor, speed controller and the battery. The performance of such a system (i.e. thrust and energy consumption as functions of airspeed) can be found by experiment in a wind tunnel, from manufacturers' brochures, or using freely available software such as MotoCalc [23]. Fig. 5 shows that the commercial MotoCalc simulation results correlate well with experimental measurements, except at airspeeds over about 18 m/s.

Moments of inertia

Another important physical parameter of an aircraft is its mass moment of inertia about the various axes. The moment of inertia can be calculated from first principles for simple geometries, or found as an output from computer-aided design (CAD) software. However, this is often very inaccurate, and the moment of inertia of a small airplane can then be determined experimentally, as next explained.

The moment of inertia of a compound assembled, semi-symmetrical object, such as the small UAV, may be measured using the bifilar pendulum method. This approach uses the period of the composite system's undamped oscillations to calculate the moment of inertia. The UAV is suspended by two cables, and then oscillated about its centre of gravity. It is important that the two cables be of equal length and hang parallel, equidistant from the object's centre of gravity. The airplane must also hang horizontally in its position of rest. Further, the length of the cables should
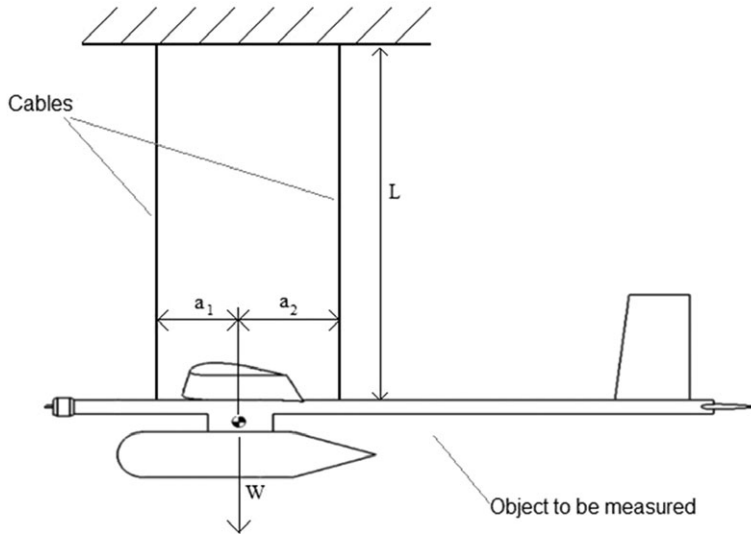
Fig. 6   *Experimental setup to measure the mass-inertia of a small airplane.*

exceed four times the distance between them, that is, with reference to Fig. 6, $L > 4(a_1 + a_2)$ [27].

The object is now rotated out of its position of rest by no more than 20° from the centre line, and then released so that a clear oscillation occurs. The period of the resulting oscillation is measured, from which the inertia can be calculated using equation 7 [27–29]:

$$I = \frac{\bar{m}g\Delta t^2 a_1 a_2}{4\pi^2 L} \qquad (7)$$

with $\bar{m}g$ the object weight (expressed in N), Δt the period of motion (s) and a_1, a_2 and L are the lengths defined in Fig. 6.

The small UAV is assumed to be symmetrical about the x–z plane (axes as defined in Fig. 2). This means that $I_{xy} = I_{xz} = I_{zy} = 0$ [21].

Flight speeds

Using AVL, data can be generated for a UAV in trimmed flight at various airspeeds (i.e. trimming the angle of attack for requisite lift, and elevator deflection to balance a pitching moment). This, along with data for available thrust at speed, can be used to choose operating speeds for conditions such as level flight, and climb/descent rate. Specifically, the stall speed and the cruising speeds for two flight conditions, maximum range and maximum flight time, can be found. For obvious reasons, the aircraft drag plays an important role in these calculations.
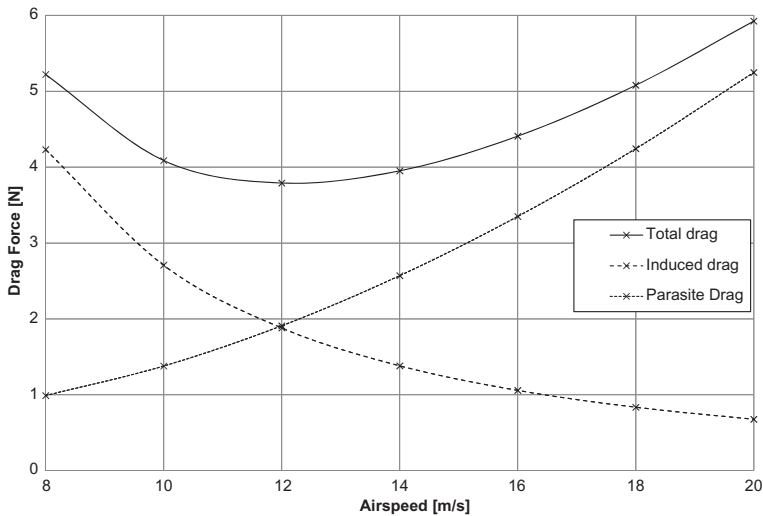
Fig. 7   *Total drag and drag components for level flight, for the experimental UAV.*

The drag is decomposed into two parts: the base drag and the induced drag
[24, 25], or $D = D_0 + D_i = qS\left(C_{D0} + \dfrac{C_L{}^2}{\pi Ae}\right)$, with the base drag ($D_0$) scaling according

to V^2, and the induced drag (D_i) as V^{-2} (Fig. 7).

Stall speed
As the speed of the aircraft decreases, the dynamic pressure also drops (since $q = 1/2(\rho V^2)$). Since the total lift generated must equal the weight during steady flight, the wing needs to be at a higher angle of attack (and thus generate a larger coefficient of lift) at lower speeds. As soon as the required local lift coefficient (C_l) over some part of the wing exceeds the aerofoil maximum lift coefficient, the wing is stalled.

The stall speed of an aircraft is therefore defined as the speed at which the required local lift coefficient at some part of the wing exceeds the aerofoil maximum lift coefficient, and is the speed below which the aircraft cannot maintain altitude. This can be found by inspection, using a program such as AVL, which estimates the span-wise lift distribution (see Fig. 8).

Speed for maximum range
For maximum range, it is required that drag force on the aircraft be a minimum (noting that work done equals force times displacement, the maximum displacement that can be obtained from a given amount of work – the batteries' capacity – will be at the minimum drag force) [24, 25]. This is, however, a somewhat simplified approach, as it neglects any speed dependence of the propulsion system.
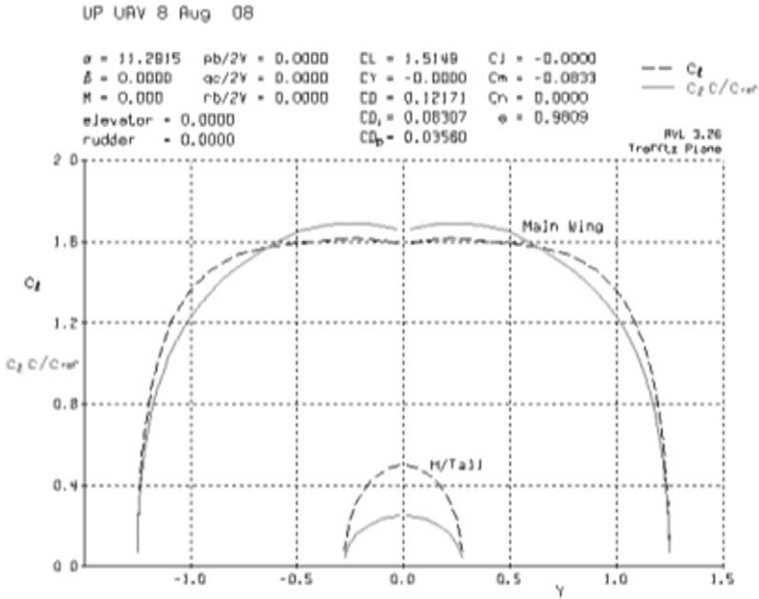
UP UAV 8 Aug 08

a = 11.2815   pb/2V = 0.0000   CL = 1.5149   Cl = -0.0000
β = 0.0000   qc/2V = 0.0000   CY = -0.0000   Cm = -0.0833
M = 0.000   rb/2V = 0.0000   CD = 0.12171   Cn = 0.0000
elevator = 0.0000   CDi = 0.08307 e = 0.9809
rudder = 0.0000   CDp = 0.03560

AVL 3.26
Trefftz Plane

Fig. 8   *AVL Trefftz plane output of the experimental UAV, showing local lifting coefficient (dashed lines) for main wing and horizontal tail for level flight at 9.7 m/s versus span (in m). Note that the main wing is stalled near mid-span (locally, $C_l > C_{l(max)} = 1.6$).*
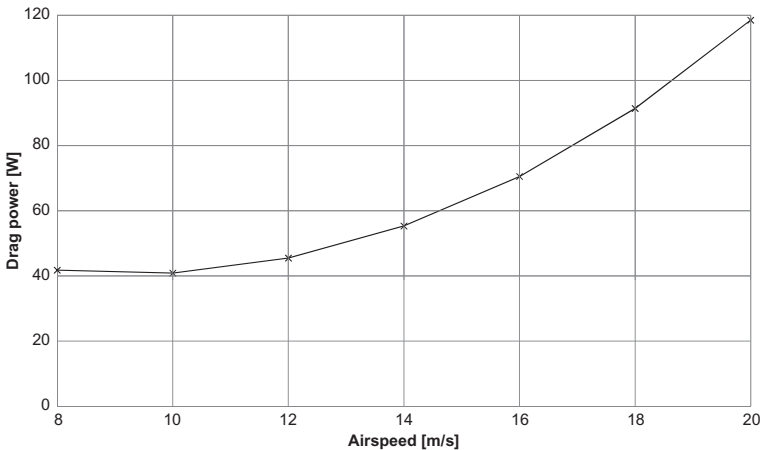

Fig. 9   *Drag power during level flight of the experimental UAV.*

Speed for maximum flight time
The maximum flight time condition (also known as the loiter speed) is that speed at which the minimum power is required for flight (i.e. at which the batteries will last the longest) and is typically lower than the speed for maximum range [24, 25]. The power required can be found with $P_{req} = DV$, and is plotted in Fig. 9.
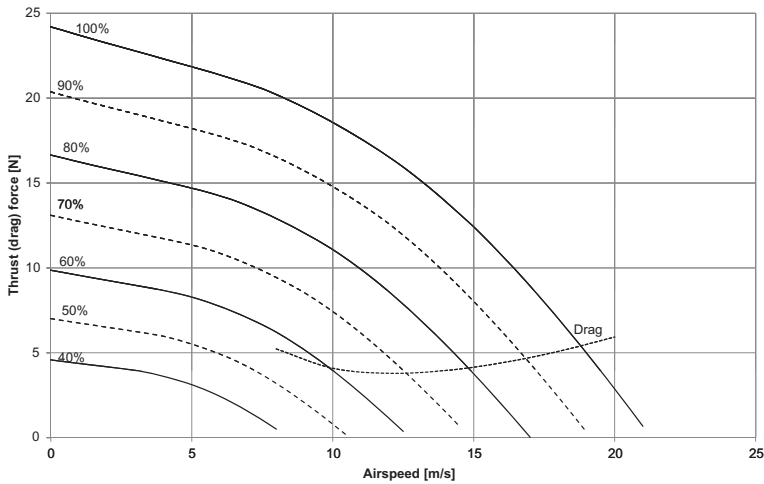
Fig. 10   *Thrust and trimmed drag forces for steady-state flight, for the experimental UAV. The throttle corresponding to each thrust curve is expressed as a percentage of maximum.*
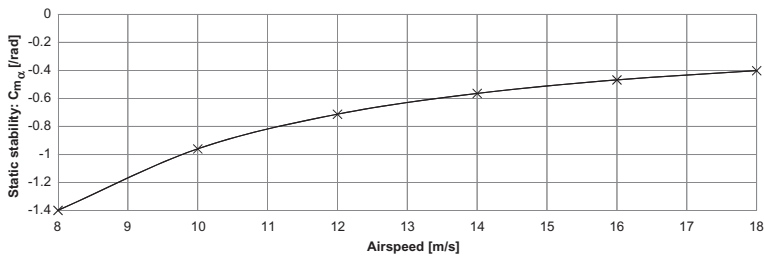

Fig. 11   *Static stability as a function of airspeed for the experimental UAV. Note that the pitch derivative remains negative, and the UAV is statically stable for all airspeeds.*

Operational flight speed and trim settings

For a typical surveillance mission, a UAV would be set up such that it flies towards the target area at the maximum-range speed (so that minimum battery power is wasted while getting to the target, thereby maximizing the time spent at the target), and then switch to the loiter speed while over the target area [30]. Returning to base it would again use maximum-range flight. However, in general, the airspeed will be chosen as a compromise between energy efficiency, time available, and desired climb/descent rate [31].

The speeds at which the UAV can operate during level flight can be found as those speeds which are above the stall speeds, and for which the maximum available thrust exceeds the drag force (see Fig. 10, from which the throttle settings for steady flight can be determined).

As the airspeed increases, the required thrust also increases, which leads to a decrease in the aircraft's static longitudinal stability (Fig. 11), due to the destabiliz-
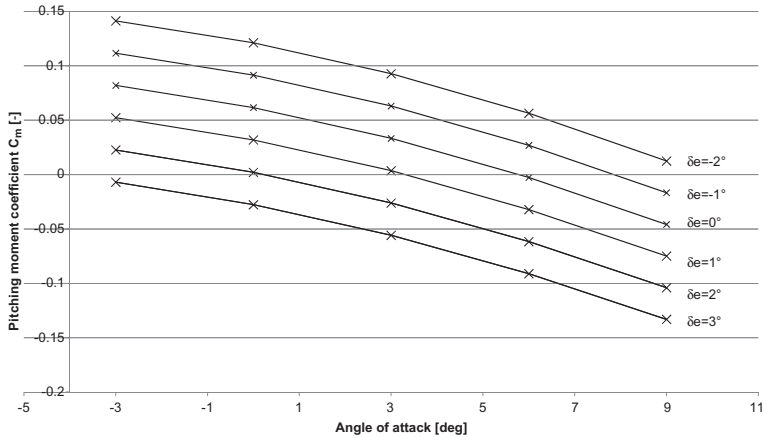
Fig. 12   *Pitch–trim plot – the trimmed elevator deflection is that which results in zero pitching moment at a specified angle of attack.*

ing nature of a tractor propeller. Also, as the airspeed changes the neutral point of the aircraft moves, due to the change in downwash at the horizontal stabilizer. It is therefore important to verify that, for all possible flight speeds, the airframe remains stable (Fig. 11).

During level flight, the elevator deflection, δ_e, is chosen so that the net pitching moment acting on the aircraft is zero. The required δ_e can be estimated by generating plots as in Fig. 12, by finding that elevator deflection which crosses the *x*-axis at the angle of attack necessary to generate enough lift to balance the weight of the UAV.

Climbing performance

During steady flight, an aircraft uses excess power to gain altitude [24,25]. The vertical speed achievable by an aircraft can be determined from the excess power available and the weight of the aircraft: $(mg)V_{climb} = P_{excess}$. The flight path angle, γ, can then be determined, assuming zero wind and noting that, for flight with zero bank angle [24, 25]:

$$\sin \gamma = \frac{V_{climb}}{V} = \frac{P_{excess}}{mgV} \tag{8}$$

Launching the UAV

Hand-launching is a popular method of launching UAVs of masses below approximately 4 kg [8]. However, for this to be safe, one needs to ensure that sufficient energy can be imparted to the UAV, in the time available. During the launch, the UAV gains momentum from the throwing action (leaving the thrower's hand at V_{launch}) and from the motor ($T\Delta t$), the sum of which has to exceed the momentum of the UAV at stall speed. Note that, in reality, the propeller thrust decreases with

airspeed, so the value used for T should be selected with care (e.g. the thrust at stall speed, as a lower limit). From this, the approximate time during which the UAV will be losing height can be found as $t_{\text{fall}} = \dfrac{m(V_{\text{stall}} - V_{\text{throw}})}{T}$, and the height through which it would fall, under the very conservative assumption of zero lift, is $\Delta y = \dfrac{1}{2} g t_{\text{fall}}^2$. If this value is less than the height from which the UAV is thrown, a hand-launch will be successful.

Alternatively, it is relatively straightforward to create a simulation of the launch process, making a simplifying assumption such as constant pitch angle, and allowing lift, drag and thrust to vary with airspeed and angle of attack.

UAV transfer functions

In the following sections the transfer functions describing the UAV response to various inputs will be derived. The transfer functions, each a ratio of polynomials in the form $G(s) = \dfrac{Y(s)}{U(s)}$, describe the (linear) relationship between a system input $u(t)$ and an output $y(t)$, and their various derivatives [32]. These functions serve two main purposes: first, the dynamic stability of the system can be determined by examining the system poles; and second, they can be used for designing an autopilot control system [33, 34].

Dimensionless coefficients and related derivatives

The numerous required aerodynamic coefficients can be obtained from wind tunnel testing, numerical computational methods, or from identification of flight test parameters [35, 36]. Many of the values can be estimated using simple equations, derived from first-principle approximations of the airframe, while other values are more difficult to estimate, and require other methods, such as empirical look-up tables or numerical simulations. Where possible, multiple methods should be used, with the resulting spread of values giving insight into the likely error being made.

Coefficients of pitching moment (C_m) and thrust (C_T)

During steady, level flight, the aircraft total pitching moment (and therefore the total pitching moment coefficient) must equal zero [36]. The total pitching moment of the aircraft is composed of the aerodynamic pitching moment ($C_{m(A)}$) due to wings, fuselage and horizontal tail, and the pitching moment due to thrust effects ($C_{m(T)}$).

The pitching moment of the propeller is due to the airflow being accelerated backwards and downwards, while flying at a non-zero angle of attack. This downwards deflection of the airflow results in an upwards reaction force on the propeller, which, coupled with the long moment arm of the thrust to the centre of gravity, results in a pitching moment [37].
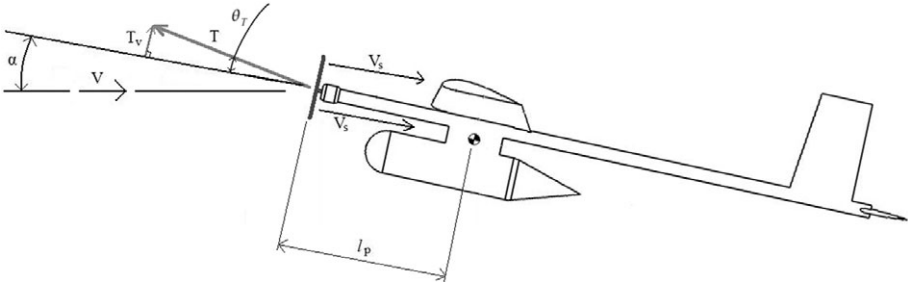
Fig. 13   *UAV travelling at speed V and positive angle of attack α, accelerating air to speed V_s through the propeller, resulting in thrust T, with perpendicular component T_v and moment arm l_p.*

To estimate the resulting moment, some assumptions are made. First, at zero angle of attack, it is assumed that the line of action of the thrust force passes through the centre of gravity. Second, at a non-zero angle of attack, it is assumed that the air is accelerated through the propeller such that it is deflected through the angle of attack, that is, ends up flowing parallel to the airframe reference frame (Fig. 13).

The thrust delivered by the propeller is solely dependent on the aerodynamics of the propeller, so the thrust force was calculated based on blade element theory [24, 38, 39]. The speed of the air accelerated through the propeller, for $\alpha = 0$, could thus be estimated from the Rankine–Froude propeller theory [30, 38, 39] by:

$$V_S = \sqrt{V^2 + \frac{2T}{\rho S_D}} \tag{9}$$

with S_D the area of the disk swept by the propeller, and V the free stream speed. Using these values, the angle θ_T was estimated with [24, 25]:

$$\tan \theta_T = \frac{V \sin \alpha}{V_S - V \cos \alpha} \tag{10}$$

The non-dimensional pitching moment coefficient due to thrust was then found to be:

$$C_{m(T)} = \frac{T l_p \sin \theta_T}{q S \bar{c}} \tag{11}$$

From the equations it can be seen that, for tractor propeller configurations, $\dfrac{\partial C_{m(T)}}{\partial \alpha} = C_{m\alpha(T)} > 0$; that is, the thrust acts to destabilize the aircraft.

As the aircraft's angle of attack changes, the lift produced by the wing and horizontal tail also changes. This change in lift, along with the moment arms through which the forces act, gives rise to a change in the aerodynamic pitching moment, which can be estimated with [25, 36]:

$$C_{m\alpha(A)} = a_w \frac{l_w}{\bar{c}} - a_t \eta_t \bar{V}_h (1 - \varepsilon_\alpha) \tag{12}$$

where the horizontal tail volume coefficient is defined as $\bar{V}_h = \frac{l_t S_t}{\bar{c} S}$.

Estimates for $C_{m_\alpha(A)}$ are also available from both Datcom and AVL, and were used to verify the hand calculations [11]. The total pitching moment for the aircraft, which determines the static stability of the aircraft in pitch, is $C_{m_\alpha} = C_{m_\alpha(A)} + C_{m_\alpha(T)}$. At low Mach numbers (below $V / V_{sound} \approx 0.4$), as is the case with the authors' UAV,

the derivative $\dfrac{\partial C_m}{\partial u}$ can be assumed negligible [25, 36].

The rate of change of angle of attack, $\dfrac{d\alpha}{dt}$, also influences the pitching moment

of the aircraft, but its effect is difficult to predict. Using the so-called 'lag of downwash' method, equation 13 was used [25, 36]. This value is also available as an output from Datcom, but not from *AVL*.

$$C_{m\dot{\alpha}} = \frac{\partial C_m}{\partial \dot{\alpha}} = -2 a_t \eta_t \bar{V}_h \frac{l_t}{\bar{c}} \varepsilon_\alpha \tag{13}$$

Pitch rate, $q = \dfrac{d\theta}{dt}$, influences the total pitching moment similarly to $\dfrac{d\alpha}{dt}$, except

that the point of rotation for pitch is the aircraft's centre of gravity, while for angle of attack the rotation point lies at $x = \infty$. The pitch damping derivative was then estimated (ignoring any contribution from the main wing) with equation 14 [26]. Both Datcom and AVL also gave estimates of this value.

$$C_{m_q} = \frac{\partial C_m}{\partial q} = -2 a_t \eta_t \bar{V}_h \frac{l_t}{\bar{c}} \tag{14}$$

Finally, the value relating elevator deflection to pitching moment ($C_{m_{\delta e}} = \dfrac{\partial C_m}{\partial \delta_e}$) was

calculated from the lift-curve slope of the horizontal stabilizer, using AVL.

The coefficient of thrust uses the diameter of the propeller and the rotational speed (in min^{-1}) to express the thrust in dimensionless form [25, 36]:

$$C_T = \frac{T}{\rho n^2 D_{prop}^4} \tag{15}$$

Also required are the derivatives of C_T with respect to forward speed, C_{T_u}; and angle of attack, C_{T_α}. These are, however, difficult to estimate, and are best found with numerical analysis [1, 7, 33, 34, 36].

Coefficient of lift (C_L)

During level, steady flight, the lift produced must equal the weight of the UAV. This fact was used to find the required lift coefficient for cruise, with:

$$C_{\text{L}} = \frac{mg}{qS} \tag{16}$$

The derivative of lift coefficient with respect to angle of attack was found using an equation similar to that for C_{m_α}, as below [25, 36]. Once again, both Datcom and AVL provided estimates for this.

$$C_{L_\alpha} = a_{\text{w}} + a_{\text{t}}\eta_{\text{t}}\frac{S_{\text{t}}}{S}(1-\varepsilon_\alpha) \tag{17}$$

The derivative with respect to flight speed was found (for a cruising Mach number $M = 0.054$) using [25, 36]:

$$C_{L_u} = \frac{M^2}{1-M^2}C_{\text{L}} \text{ for } V/V_{\text{sound}} < 0.4 \tag{18}$$

The two rate derivatives, C_{L_q} and $C_{L_{\dot\alpha}}$, were found using the following equations [25, 36]:

$$C_{L_{\dot\alpha}} = 2a_{\text{t}}\eta_{\text{t}}\bar{V}_{\text{h}}\varepsilon_\alpha \tag{19}$$

$$C_{L_q} = 2a_{\text{t}}\eta_{\text{t}}\bar{V}_{\text{h}} \tag{20}$$

The effect of elevator deflection on C_{L} can be estimated using AVL. However, in the case of the authors' UAV, where the elevator is much smaller than the main wing, C_{L} was assumed to be a negligible quantity.

Coefficient of drag (C_D)

The zero-lift drag coefficient C_{D0} is defined as the drag of the aircraft while zero lift is produced. From this, the drag at different flight conditions was estimated using

$C_{\text{D}} = C_{\text{D0}} + \dfrac{C_{\text{L}}^2}{\pi Ae}$, with e being the Oswald efficiency and $\dfrac{C_{\text{L}}^2}{\pi Ae}$ the induced drag.

C_{D0} is another difficult parameter to estimate, and is best found using wind tunnel tests. It can also be estimated by hand using a drag breakdown, CFD analysis, or Datcom. The authors used Datcom to estimate it. The derivative with respect to angle of attack was found with [25, 36]:

$$C_{D_\alpha} = \frac{2C_{\text{L}}C_{L_\alpha}}{\pi Ae} \tag{21}$$

At low Mach numbers (below 0.4), the drag coefficient is approximately independent of speed [9,12], or, $C_{D_u} = \dfrac{\partial C_{\text{D}}}{\partial u} \approx 0$.

The derivative of C_D with respect to an elevator deflection was again found using AVL.

Dimensional stability derivatives

To assemble the longitudinal transfer functions, it is necessary to convert the dimensionless coefficients calculated above to dimensional coefficients. These derivatives are derived such that the derivative represents the linear (or angular) acceleration imparted to the airplane as a result of a unit change in its associated motion or control variable [13,35]. For example, the dimensionless coefficient C_{m_α} was rewritten to give $\dfrac{q_1 S \overline{c} C_{m_\alpha} \alpha}{I_{yy}} = M_\alpha \alpha$, where M_α represents the pitch angular acceleration imparted to the airplane as a result of a unit change in angle of attack. The dimensional stability derivatives were then calculated according to the following list, with a subscript one ($_1$) indicating the nominal value, for example u_1 being the nominal flight speed [25, 36]:

$$X_u = -\frac{q_1 S (C_{D_u} + 2C_{D_1})}{\overline{m} u_1} \tag{22}$$

$$X_{Tu} = \frac{q_1 S (C_{T_{xu}} + 2C_{T_1})}{\overline{m} u_1} \tag{23}$$

$$X_\alpha = -\frac{q_1 S (C_{D_\alpha} - C_{L_1})}{\overline{m}} \tag{24}$$

$$X_{\delta e} = -\frac{q_1 S C_{D_{\delta e}}}{\overline{m}} \tag{25}$$

$$Z_u = -\frac{q_1 S (C_{L_u} + 2C_{L_1})}{\overline{m} u_1} \tag{26}$$

$$Z_\alpha = -\frac{q_1 S (C_{L_\alpha} + 2C_{D_1})}{\overline{m}} \tag{27}$$

$$Z_\alpha = -\frac{q_1 S \overline{c} C_{L_\alpha}}{2 \overline{m} u_1} \tag{28}$$

$$Z_q = -\frac{q_1 S \overline{c} C_{L_q}}{2 \overline{m} u_1} \tag{29}$$

$$Z_{\delta e} = -\frac{q_1 S C_{L_{\delta e}}}{\overline{m}} \tag{30}$$

$$M_u = \frac{q_1 S \overline{c} (C_{m_u} + 2C_{m_1})}{I_{yy} u_1} \tag{31}$$

$$M_{Tu} = \frac{q_1 S \overline{c} (C_{m_{Tu}} + 2C_{m_{T_1}})}{I_{yy} u_1} \tag{32}$$

$$M_\alpha = \frac{q_1 S \overline{c} C_{m_\alpha}}{I_{yy}} \tag{33}$$

$$M_{T\alpha} = \frac{q_1 S \overline{c} C_{m_{T\alpha}}}{I_{yy}} \tag{34}$$

$$M_\alpha = \frac{q_1 S \overline{c}^2 C_{m_\alpha}}{2 I_{yy} u_1} \tag{35}$$

$$M_q = \frac{q_1 S \overline{c}^2 C_{m_q}}{2 I_{yy} u_1} \tag{36}$$

$$M_{\delta e} = \frac{q_1 S \overline{c} C_{m_{\delta e}}}{I_{yy}} \tag{37}$$

Longitudinal transfer functions
Assembling the transfer functions

The longitudinal open-loop transfer functions $\dfrac{U(s)}{\delta_e(s)}$, $\dfrac{\alpha(s)}{\delta_e(s)}$ and $\dfrac{\theta(s)}{\delta_e(s)}$ could then

be assembled, using equations of following form:

$$\frac{U(s)}{\delta e(s)} = \frac{N_u(s)}{\overline{D}_1(s)}$$

With $\overline{D}_1(s)$ the denominator common to all three transfer functions $\overline{D}_1(s) = A_1 s^4 + B_1 s^3 + C_1 s^2 + D_1 s + E_1$, and $N_u(s) = A_u s^4 + B_u s^3 + C_u s^2 + D_u s + E_u$ the numerator of the transfer function. The numerators for $\dfrac{\alpha(s)}{\delta e(s)}$ and $\dfrac{\theta(s)}{\delta e(s)}$ are denoted $N_\alpha(s) = A_\alpha s^3 + B_\alpha s^2 + C_\alpha s + D_\alpha$ and $N_\theta(s) = A_\theta s^2 + B_\theta s + C_\theta$, respectively.

The values for all the coefficients were calculated as shown below, where the numerical values are the solution when the dimensional derivatives calculated are substituted [25, 36]:

$$A_1 = U_1 - Z_\alpha \tag{38}$$

$$B_1 = -(U_1 - Z_\alpha)(X_u + X_{Tu} + M_q) - Z_\alpha - M_\alpha(U_1 + Z_q) \tag{39}$$

$$
\begin{aligned}
C_1 = {}& (X_u + X_{Tu})(M_q(U_1 - Z_\alpha) + Z_\alpha + M_\alpha(U_1 + Z_q)) + \\
& M_q Z_\alpha - Z_u X_\alpha + M_\alpha g \sin\theta_1 - (M_\alpha + M_{T\alpha})(U_1 + Z_q)
\end{aligned} \tag{40}
$$

$$
\begin{aligned}
D_1 = {}& g\sin\theta_1 (M_\alpha + M_{T\alpha} - M_\alpha(X_u + X_{Tu})) + \\
& g\cos\theta_1 (Z_u M_\alpha + (M_U + M_{Tu})) + \\
& (M_U + M_{Tu})(-X_\alpha(U_1 + Z_q)) + Z_u X_\alpha M_q + \\
& (X_U + X_{Tu})((M_\alpha + M_{T\alpha})(U_1 + Z_q) - M_q Z_\alpha)
\end{aligned} \tag{41}
$$

$$E_1 = g\sin\theta_1\left((M_u + M_{\mathrm{T}u})X_\alpha - (X_u + X_{\mathrm{T}u})(M_\alpha + M_{\mathrm{T}\alpha})\right) +$$
$$g\cos\theta_1\left((M_\alpha + M_{\mathrm{T}\alpha})Z_u - (M_u + M_{\mathrm{T}u})Z_\alpha\right) \tag{42}$$

$$A_u = X_{\delta e}(U_1 - Z_\alpha) \tag{43}$$

$$B_u = -X_{\delta e}\left((U_1 - Z_\alpha)M_q + Z_\alpha + M_\alpha(U_1 + Z_q)\right) + Z_{\delta e}X_\alpha \tag{44}$$

$$C_u = X_{\delta e}\left(M_q Z_\alpha + M_\alpha g\sin\theta_1 - (M_\alpha + M_{\mathrm{T}\alpha})(U_1 + Z_q)\right) -$$
$$Z_{\delta e}\left(M_\alpha g\cos\theta_1 + X_\alpha M_q\right) + M_{\delta e}\left(X_\alpha(U_1 + Z_q) - (U_1 - Z_\alpha)g\cos\theta_1\right) \tag{45}$$

$$D_u = X_{\delta e}(M_\alpha + M_{\mathrm{T}\alpha})g\sin\theta_1 - Z_{\delta e}M_\alpha g\cos\theta_1 + M_{\delta e}(Z_\alpha g\cos\theta_1 - X_\alpha g\sin\theta_1) \tag{46}$$

$$A_\alpha = Z_{\delta e} \tag{47}$$

$$B_\alpha = X_{\delta e}Z_u + Z_{\delta e}\left(-M_q - (X_u + X_{\mathrm{T}u})\right) + M_{\delta e}(U_1 + Z_q) \tag{48}$$

$$C_\alpha = X_{\delta e}\left((U_1 + Z_q)(M_u + M_{\mathrm{T}u}) - M_q Z_u\right) + Z_{\delta e}M_q(X_u + X_{\mathrm{T}u}) +$$
$$M_{\delta e}\left(-g\sin\theta_1 - (U_1 + Z_q)(X_u - X_{\mathrm{T}u})\right) \tag{49}$$

$$D_\alpha = -X_{\delta e}(M_u + M_{\mathrm{T}u})g\sin\theta_1 + Z_{\delta e}(M_u + M_{\mathrm{T}u})g\cos\theta_1 +$$
$$M_{\delta e}\left((X_u + X_{\mathrm{T}u})g\sin\theta_1 - Z_u g\cos\theta_1\right) \tag{50}$$

$$A_\theta = Z_{\delta e}M_\alpha + M_{\delta e}(U_1 - Z_\alpha) \tag{51}$$

$$B_\theta = X_{\delta e}\left(Z_u M_\alpha + (U_1 - Z_\alpha)(M_u + M_{\mathrm{T}u})\right) +$$
$$Z_{\delta e}\left((M_\alpha + M_{\mathrm{T}\alpha}) - M_\alpha(X_u + X_{\mathrm{T}u})\right) +$$
$$M_{\delta e}\left(-Z_\alpha - (U_1 - Z_\alpha)(X_u + X_{\mathrm{T}u})\right) \tag{52}$$

$$C_\theta = X_{\delta e}\left((M_\alpha + M_{\mathrm{T}\alpha})Z_u - (M_u + M_{\mathrm{T}u})Z_\alpha\right) +$$
$$M_{\delta e}\left(Z_\alpha(X_u + X_{\mathrm{T}u}) - X_\alpha Z_u\right) +$$
$$Z_{\delta e}\begin{pmatrix}-(M_\alpha + M_{\mathrm{T}\alpha})(X_u + X_{\mathrm{T}u}) + \\ X_\alpha(M_u + M_{\mathrm{T}u})\end{pmatrix} \tag{53}$$

System poles and modes

The denominator $\bar{D}_1(s)$ is of key interest as it determines the poles of the system, which govern the dynamic stability. The system is asymptotically stable if and only if all the poles (that is, the solutions for $\bar{D}_1(s) = 0$) lie strictly on the left of the imaginary axis in the complex plane [32].

The system poles were used to determine the natural frequency and damping ratios of the *short period* and *phugoid* modes (Fig. 14). As the name implies, the short period is the mode with the higher natural frequency, and is a mode consisting mainly of a variation in θ and α, with the forward speed, U, remaining approximately constant. The short period mode is typically well damped, with a scale of motion approximately two orders of magnitude lower than that of the phugoid mode. The phugoid mode excites mainly the pitch angle and forward speed, with angle of attack approximately constant [1–7]. These dynamic modes provide important characterizations of the airplane's handling qualities, which are not treated in this paper.
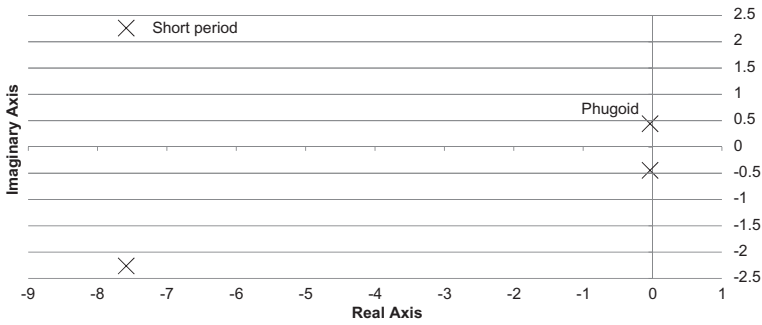
Fig. 14   *Location of system poles on the s-plane for the experimental UAV, indicating which poles account for the short period and phugoid modes, with all poles being stable, indicating the UAV is dynamically stable.*

TABLE 2   *Dynamic results for the experimental UAV*

Parameter	Value
Equilibrium flight condition	$U = 18 \ m/s$ $\alpha = negative$ $h = m$
Transfer function: elevator defletion to forward speed	$\dfrac{U(s)}{\delta e(s)} = \dfrac{-0.08075(s-64.7332)(s+62.9769)(s+16.9442)}{s^4 + 15.25s^3 + 64.03s^2 + 7.695s + 12.41}$
Transfer function: elevator defletion to angle of attack	$\dfrac{U(s)}{\alpha(s)} = \dfrac{-78.56(s^2 + 0.0634s + 0.6311)}{s^4 + 15.25s^3 + 64.03s^2 + 7.695s + 12.41}$
Transfer function: elevator defletion to pitch angle	$\dfrac{U(s)}{\theta(s)} = \dfrac{-84.45(s+6.6755)(s+0.6311)}{s^4 + 15.25s^3 + 64.03s^2 + 7.695s + 12.41}$
System poles	$s = -7.588 \pm 2.2612i$ $s = -0.0374 \pm 0.4432i$
Phugoid mode characteristics	$\bar{\omega}_n = 0.1978 \ rad / s$ $\varsigma = 0.08409 \ rad / s$
Short period mode characteristics	$\bar{\omega}_n = 7.92 \ rad / s$ $\varsigma = 0.959 \ rad / s$

Typical results

The consolidated results obtained for the experimental UAV are given in Table 2. The most important result is that all the system poles have negative real parts, meaning that the system is asymptotically stable, that is, it will reject small disturbances around the equilibrium. The successful (stable) flight of the UAV corroborated these findings.

Some information about the flying qualities of the UAV was also determined by investigating the period and damping ratio of the longitudinal modes. These values can also be used for subsequent autopilot design.

Conclusion

A simple mini-UAV has been built and subjected to wind tunnel and other testing. Freely available software has been used to assist with the dynamic characterization of the airplane, specifically with respect to longitudinal dynamics.

The use of freely available software fulfils in the requirements of lay design engineers or engineering students venturing into the field of UAV design and testing, who require cheap and quick, though acceptable estimations of the open-loop longitudinal dynamics of a small UAV. The simulation data were used to prepare dimensional stability derivatives, from which longitudinal transfer functions were produced. These, in turn, were used to estimate the dynamic characteristics of the UAV, which could preempt subsequent autopilot design and further wind tunnel testing.

The paper presents theory and results in such a format that would hopefully be beneficial to research engineers and engineering students with limited aeronautical training or experience. Based on their analyses and validation work, the authors strongly recommend the use of the freely available software Datcom+, AVL, XFLR5, and MotoCalc, for conceptual dynamic characterization of a UAV.

Acknowledgements

References

[1] R. C. Nelson, *Flight Stability and Automatic Control* (McGraw-Hill, New York, 1997).
[2] J. Roskam, *Airplane Flight Dynamics and Automatic Flight Controls, Parts I and II* (DARCorporation, Lawrence, KA, 1998).
[3] M. V. Cook, *Flight Dynamics Principles* (John Wiley & Sons, New York, 1997).
[4] B. Etkin, *Dynamics of Flight: Stability and Control* (John Wiley & Sons, New York, 1996).

[5] B. L. Stevens and F. L. Lewis, *Aircraft Control and Simulation* (John Wiley & Sons, Hobokren, NJ, 2003).

[6] R. F. Stengel, *Flight Dynamics* (Princeton University Press, Princeton, NJ, 2004).

[7] D. McRuer, I. Ashkensas and D. Graham, *Aircraft Dynamics and Automatic Control* (Princeton University Press, Princeton, NJ, 1973).

[8] K. Valavanis and K. P. Valavanis, *Advances in Unmanned Aerial Vehicles: State of the Art and the Road to Autonomy* (Springer, Dordrecht, 2007).

[9] D. Jung, J. Ratti and P. Tsiotras, 'Real-time implementation and validation of a new hierarchical path planning scheme of UAVs via hardware-in-the-loop simulation', *J. Intell. Robot Syst.*, **54** (2009), 163–181.

[10] H. Chao, Y. Cao and Y. Chen, 'Autopilots for small fixed-wing unmanned aerial vehicles: a survey', *Int. J. Contr. Automat. Syst.*, **8**(1) (2010), 36–44.

[11] Anon., 'Flight at small scale takes off', Innovate, no. 3 (2009), 83, available at http://web.up.ac.za/sitefiles/file/44/2163/8121/Innovate%203/Inn%20bl80-83.pdf (accessed 1 July 2011).

[12] D. Jung and P. Tsiotras, 'Modeling and hardware-in-the-loop simulation for a small unmanned aerial vehicle', in *AIAA Infotech at Aerospace, AIAA 07–2763* (American Institute of Aeronautics and Astronautics, Rohnert Park, May 2007).

[13] R. D. Finck, *US Air Force Stability and Control Data Compendium (Datcom)* (DARCorporation, Lawrence, KS, 1983).

[14] J. E. Williams and S. R. Vukelich, *The USAF Stability and Control DATCOM: AFFDL-TR-79–3032* (McDonnell Douglas Aircraft Corporation, St Louis, MO, 1979).

[15] M. Drela and H. Youngren, *Athena Vortex Lattice (AVL)* (Massachusetts Institute of Technology, Department of Aeronautical and Astronautical Engineering), available at http://web.mit.edu/drela/Public/web/avl/ (accessed 10 March 2008).

[16] XFLR5, Analysis tools for airfoils, available at http://sourceforge.net/projects/xflr5/ (accessed March 2008).

[17] M. C. Shields, C. M. Hatcher, R. A. Pitcairn, C. W. Aiken, D. B. Berman, C. M. Carnahan, W. A. Foley, S. P. Hammervold, W. E. Holway and L. C. Marek, *Design and Development of a Reconnaissance Micro Air Vehicle and Launch System*, available at http://www.colorado.edu/ASEN/SrProjects/Archive/AIAA_Paper_Awards/MARVLIS_AIAA_Final.pdf (accessed 12 July 2011).

[18] K. C. Stewart, K. Blackburn, J. Wagener, J. Czabarane and G. Abate, *Development and Initial Flight Tests of a Single-Jointed Articulated-Wing Micro Air Vehicle, AIAA 2008–6708* (AIAA Atmospheric Flight Mechanics Conference and Exhibit, Reston, VA, 2008).

[19] R. L. Pereira. *Validation of Software for the Calculation of Aerodynamic Coefficients* (bachelor's dissertation, Department of Management and Engineering, Linköping University, 2010), available at http://scholar.google.co.za/scholar?hl=en&q=Athena+Vortex+Lattice+method+for+low+reynolds+number+work&btnG=Search&as_sdt=0%2C5&as_ylo=&as_vis=0 (accessed 12 July 2011).

[20] V. Klein, P. C. Murphy, T. J. Curry and J. M. Brandon, *Analysis of Wind Tunnel Longitudinal Static and Oscillatory Data of the F-16XL Aircraft* (NASA/TM-97–206276, 1997).

[21] V. Klein and P. C. Murphy, *Estimation of Aircraft Nonlinear Unsteady Parameters from Wind Tunnel Data* (NASA TM-1998–208969, 1998).

[22] Y. C. Paw, *Synthesis and Validation of Flight Control for UAV* (PhD thesis, Graduate School of the University of Minnesota, 2009).

[23] MotoCalc, Homepage of MotoCalc electrical propulsion system simulation, at http://www.motocalc.com (accessed 15 March 2008).

[24] B. W. McCormick, *Aerodynamics, Aeronautics and Flight Mechanics* (John Wiley & Sons, New York, 1995).

[25] J. Roskam, *Airplane Design, Part VII: Determination of Stability, Control, and Performance Characteristics: FAR and Military Requirements* (DARCorporation, Lawrence, KA, 2002).

[26] F. M. White, *Fluid Mechanics*, 5th edition (McGraw-Hill, New York, 1997).

[27] W. Gracey, *The Experimental Determination of the Moments of Inertia of Airplanes by a Simplified Compound-Pendulum Method*, report no. A574183 (NASA, Washington, DC, 1983).

[28] S. Hall, 'Dynamic modelling', *Sport Aviation* (July 1987), 30–36.

[29] T. G. Gainer and S. Hoffman, *Summary of Transformation Equations and Equations of Motion Used in Free Flight and Wind Tunnel Data Reduction Analysis* (NASA SP-3070, 1972).

[30] P. Cosyn and J. Vierendeels, 'Design of fixed wing micro air vehicles', *Aeronautical Journal* (2007), 315–326.

[31] D. P. Raymer, *Aircraft Design: A Conceptual Approach* (American Institute of Aeronautics and Astronautics, Washington, DC, 1989).

[32] G. F. Franklin, J. D. Powell and A. Emami-Naeni, *Feedback Control of Dynamic Systems* (Prentice Hall, New York, 2002).

[33] M. R. Waszak, L. N. Jenkins and P. Ifju. *Stability and Control Properties of an Aeroelastic Fixed Wing Micro Aerial Vehicle* (AIAA-2001–4005, 2001).

[34] E. C. Papageorgiou, *Development of a Dynamic Model for a UAV* (master's dissertation, Naval Postgraduate School, Monterey, CA, 1997).

[35] W. B. Blake, 'Prediction of fighter aircraft dynamic derivatives using Digital Datcom', *Proceeding of the 3rd Applied Aerodynamics Conference* (Colorado Springs, CO, AIAA-1985–4070, 1985).

[36] J. H. Blakelock, *Automatic Control of Aircrafts and Missiles* (Wiley, New York, 1991).

[37] J. Roskam, *Airplane Design, Part II: Preliminary Configuration Design and Integration of the Propulsion System* (DARCorporation, Lawrence, KA, 1997).

[38] C. N. Adkins and R. H. Liebeck, 'Design of optimum propellers'*, Journal of Propulsion and Power*, **10**(5) (1994), 676–682.

[39] T. J. Mueller and J. D. DeLaurier, 'Aerodynamics of small vehicles'*, Annual Review of Fluid Mechanics*, **35** (2003), 89–111.